

Domain Adversarial RetinaNet as a Reference Algorithm for the MITosis DOmain Generalization Challenge

Frauke Wilm¹[0000-0002-9065-0554], Christian Marzahl¹[0000-0001-9340-9873],
Katharina Breining²[0000-0001-7600-5869], and Marc
Aubreville³[0000-0002-5294-5247]

¹ Pattern Recognition Lab, Computer Sciences, Friedrich-Alexander-Universität,
Erlangen-Nürnberg, Germany

² Department of Artificial Intelligence in Biomedical Engineering,
Friedrich-Alexander-Universität, Erlangen-Nürnberg, Germany

³ Technische Hochschule Ingolstadt, Ingolstadt, Germany

Abstract. Assessing the mitotic count has a known high degree of intra- and inter-rater variability. Computer-aided systems have proven to decrease this variability and reduce labeling time. These systems, however, are generally highly dependent on their training domain and show poor applicability to unseen domains. In histopathology, these domain shifts can result from various sources, including different slide scanning systems used to digitize histologic samples. The MITosis DOmain Generalization challenge focused on this specific domain shift for the task of mitotic figure detection. This work presents a mitotic figure detection algorithm developed as a baseline for the challenge, based on domain adversarial training. On the challenge’s test set, the algorithm scored an F_1 score of 0.7183. The corresponding network weights and code for implementing the network are made publicly available.

Keywords: MIDOG · Domain Shift · Mitotic Count · Histopathology · Object Detection

1 Introduction

A well-established method of assessing tumor proliferation is the mitotic count (MC) [12] - a quantification of mitotic figures in a selected field of interest. Identifying mitotic figures, however, is prone to a high level of intra- and inter-observer variability [3]. Recent work has shown that deep learning-based algorithms can guide pathologists during MC assessment and lead to faster and more accurate results [3]. However, these algorithmic solutions are highly domain-dependent and performance significantly decreases when applying these algorithms to data from unseen domains [7]. In histopathology, domain shifts are often attributed to varying sample preparation or staining protocols used at different laboratories. These domain shifts and their impact on the resulting performance of an

algorithm have been tackled with a wide range of strategies, e.g. stain normalization [9], stain augmentation [14], and domain adversarial training [7]. Domain shifts, however, cannot only be attributed to staining variations but can also include variations induced by different slide scanners [2]. The MITosis DOmain Generalization (MIDOG) challenge [1], hosted as a satellite event of the 24th International Conference on Medical Image Computing and Computer Assisted Intervention (MICCAI) 2021, addresses this topic in the form of assessing the MC on a multi-scanner dataset. This work presents the reference algorithm developed out-of-competition as a baseline for the MIDOG challenge. The RetinaNet-based architecture was trained in a domain adversarial fashion and scored an F_1 score of 0.7183 on the final test set.

2 Material and Methods

The reference algorithm was developed on the official training subset of the MIDOG dataset [4]. We did not use any additional datasets and had no access to the (preliminary) test set during method development. The algorithm is based on a publicly available implementation of RetinaNet [10] which was extended by a domain classification path to enable domain adversarial training.

2.1 Dataset

The MIDOG training subset consists of Whole Slide Images (WSIs) from 200 human breast cancer tissue samples stained with routine Hematoxylin & Eosin (H&E) dye. The samples were digitized with four slide scanning systems: the Hamamatsu XR, the Hamamatsu S360, the Aperio CS2, and the Leica GT450, resulting in 50 WSIs per scanner. For the slides of three scanners, a selected field of interest sized approximately 2 mm^2 (equivalent to ten high power fields) was annotated for mitotic figures and hard negative look-alikes. These annotations were collected in a multi-expert blinded set-up. Aiming to support unsupervised domain adaptation approaches, no annotations were available for the Leica GT450 so that participants could only use the images for learning a visual representation of the scanner. Figure 1 illustrates exemplary patches of the scanners included in the training set.

The preliminary test set consists of five WSIs each for four slide scanning systems: the Hamamatsu XR and the Leica GT450, which already contributed to the training set, and the 3DHISTECH PANNORAMIC 1000 and the Hamamatsu RS, which were not seen during training. The scanner models of the preliminary test set, however, were undisclosed for the duration of the challenge. Participants only knew that the preliminary test set consisted of two seen and two unseen domains. This preliminary test set was used for evaluating the algorithms before submission and publishing preliminary results on a leaderboard on Grand Challenge¹. The evaluation on Grand Challenge ensured that the participants had no access to test images during method development. This restriction

¹ <https://midog2021.grand-challenge.org/>

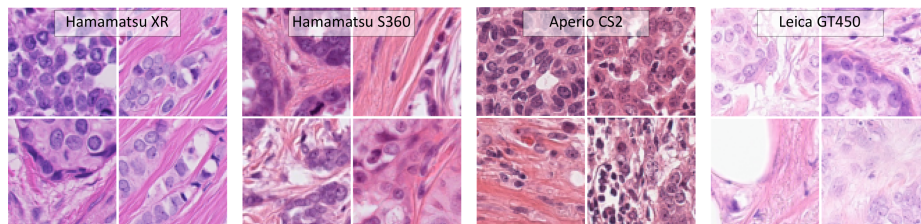


Fig. 1: Exemplary patches from the MITosis DDomain Generalization (MIDOG) challenge. Figure reproduced with permission from Aubreville *et al.* [2].

was also followed for developing the baseline algorithm. The final test set consists of 20 additional WSIs from the same scanners used for the preliminary test set. After the submission deadline, all algorithms were deployed once on this final test set for method comparison.

2.2 Domain Adversarial RetinaNet

For the domain adversarial training, we customized a publicly available RetinaNet implementation [10] by adding a Gradient Reversal Layer (GRL) and a domain classifier. For the encoder, we used a ResNet18 backbone pre-trained on ImageNet. For the domain discriminator, we were inspired by the work of Pasqualino *et al.* [13] and likewise chose three repetitions of a sequence of a convolutional layer, batch normalization, ReLU activation, and Dropout, followed by an adaptive average pooling and a fully connected layer. Implementation details can be obtained from our GitHub repository. We experimented with varying the number and positions of the domain classifier but ultimately decided for positioning a single discriminator at the bottleneck of the encoding branch. Figure 2 schematically visualizes the modified architecture.

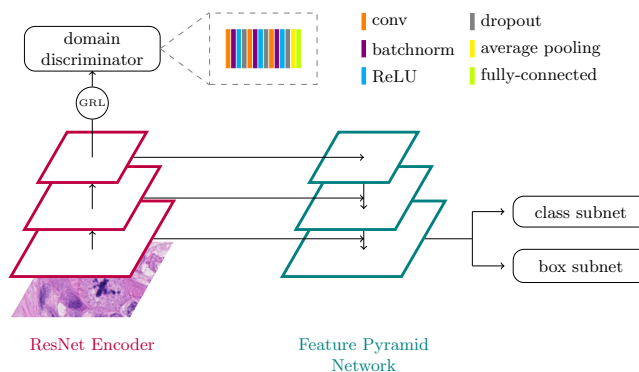


Fig. 2: Domain adversarial RetinaNet architecture.

2.3 Network Training

We split our training data into 40 training and ten validation WSIs per scanner and ensured a similar distribution of high and low MC samples in each subset. For network training, we used a patch size of 512×512 pixels and a batch size of 12. Each batch contained three images of each scanner. To overcome class imbalance, we employed a custom patch sampling, where half of the training patches were sampled randomly from the slides and the other half was sampled in a 512-pixel radius around a randomly chosen mitotic figure. Furthermore, we performed online data augmentation with random flipping, affine transformations, and random lightning and contrast change. The loss was computed as the sum of the domain classification loss for all scanners and the bounding box regression and instance classification loss for all annotated scanners:

$$\mathcal{L} = \sum_{s \in S} \frac{1}{M_s} \sum_{m=1}^{M_s} \mathcal{L}_{\text{dom},m} + \beta(s) \cdot (\mathcal{L}_{\text{bb},m} + \mathcal{L}_{\text{inst},m}) \quad \beta(s) = \begin{cases} 0, & \text{if } s = \text{GT450.} \\ 1, & \text{otherwise.} \end{cases}$$

S : set of scanners M : samples in batch

The bounding box loss \mathcal{L}_{bb} was computed as smooth L1 loss and the focal loss [8] function was used for both, the instance ($\mathcal{L}_{\text{inst}}$) and the domain (\mathcal{L}_{dom}) classification loss. During backpropagation, the gradient was negated by the GRL and multiplied with α , a weighting factor which was gradually increased from 0 to 1 following the exponential update scheme of Ganin *et al.* [6]. We trained the network with a cyclical maximal learning rate of 10^{-4} for 200 epochs until convergence. Model selection was guided by the highest performance on the validation set as well as the highest domain confusion, i.e. highest domain classification loss, to ensure domain independence of the computed features.

2.4 Evaluation

The training procedure described in the previous section was repeated three times and the validation slides of the three annotated scanners were used for performance assessment. To compare results across different model operating points, we constructed precision-recall curves and compared the area under the precision-recall curves (AUCPRs) averaged over all three scanners for which mitotic figure annotations were available. As our final model, we selected the model with the highest mean AUCPR on the validation set and selected the operating point according to the highest mean F_1 score. This resulted in a mean AUCPR of 0.7551 and an F_1 score of 0.7369 at an operating point of 0.64 on our internal validation set. This model was submitted as a reference approach to the MIDOG challenge and was evaluated using a Docker-based submission system that ensured that participants of the challenge did not have access to the test images at any time during the challenge. Before the evaluation on the final test set, we ensured the sanity of the baseline algorithm by applying the model to

the preliminary test set, which resulted in an F_1 score of 0.7401. This evaluation was run once, i.e., no hyperparameters were tuned on the preliminary test set.

For quantitative evaluation, we computed the F_1 score for mitosis detection on the challenge test set and compared the performance of the “reference approach”, trained with domain adversarial training, to a “weak baseline” trained without normalization or augmentation and a “strong baseline” trained with normalized images and the same online data augmentation methods as described in Section 2.3 but without methods for domain adaptation.

3 Results and Discussion

Across all test images, our weak baseline scored an F_1 score of 0.6279, our strong baseline an F_1 score of 0.6982, and our reference approach an F_1 score of 0.7183. Detailed results for precision, recall, and F_1 scores of the three models by scanner are summarized in Table 1. They show that the improved F_1 score over the strong baseline could mainly be attributed to a higher recall, i.e. less mitotic figures were overlooked, while precision values were very similar for most scanners.

Table 1: Performance metrics per model and scanner. The Hamamatsu XR also contributed to the training set with labeled images and the Leica GT450 with unlabeled images. The other scanners were unseen during training.

	Precision			Recall			F_1 score		
	Weak Baseline	Strong Baseline	Reference Approach	Weak Baseline	Strong Baseline	Reference Approach	Weak Baseline	Strong Baseline	Reference Approach
Seen Domains									
XR	0.8043	0.7778	0.7678	0.7291	0.7586	0.7980	0.7649	0.7681	0.7826
GT450	0.9016	0.7360	0.7318	0.2792	0.6650	0.6650	0.4264	0.6987	0.6968
Unseen Domains									
PANNORAMIC 1000	0.6698	0.5692	0.6723	0.7172	0.7475	0.8081	0.6927	0.6463	0.7339
RS	0.6559	0.6417	0.6364	0.4919	0.6210	0.6210	0.5622	0.6311	0.6286
All Scanners	0.7545	0.6965	0.7143	0.5377	0.6998	0.7223	0.6279	0.6982	0.7183

In Figure 3a, we used bootstrapping to visualize the distribution of F_1 scores per scanner. The results show that the weak baseline performed particularly badly for the Leica GT450 scanner with an average F_1 score of 0.4264 and a high variance in performance across all test slides, which becomes apparent by the wide distribution in the bootstrapping visualization. Looking at the detailed results in Table 1, this was mainly attributed to a low recall, i.e. a lot of mitotic figures were overlooked. Considering the example patches of the Leica scanner shown in Figure 1, this result is not surprising, as the Leica scanner produces images with a much higher illumination and less contrast compared to the other scanners. Without normalization, these images can challenge the network, especially since the Leica scanner was not seen during training of the baseline models due to missing annotations and was only used for training the domain generalization component of the domain adversarial network. When comparing the strong baseline with our reference approach, the models show very similar performance for most of the scanners except for the unseen PANORAMIC 1000,

where the domain adversarial training significantly increased the F_1 score to 0.7339 compared to an F_1 score of 0.6463 for the strong baseline. Furthermore, the narrower distributions of the bootstrapping in Figure 3d indicate a lower variance in performance compared to the wider distributions of the baseline models in Figures 3b and 3c.

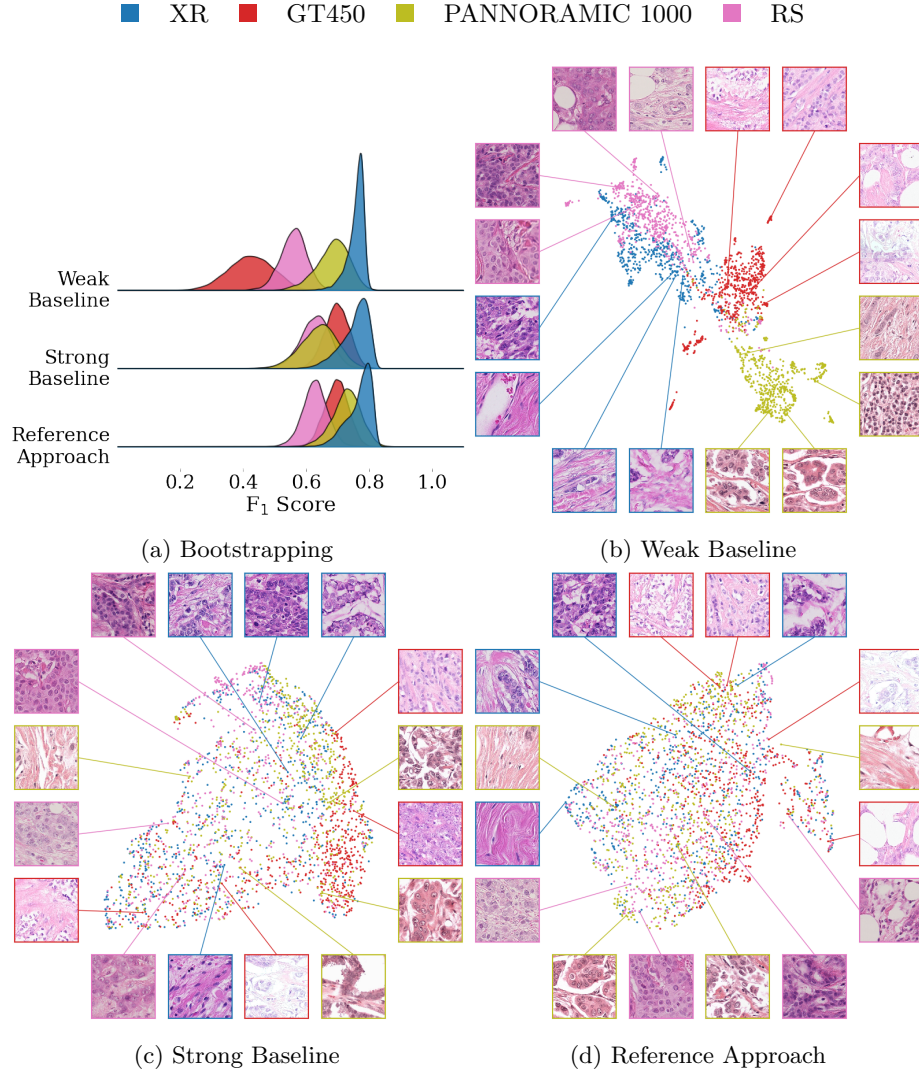


Fig. 3: Bootstrapping and Uniform Manifold Approximation and Projection (UMAP) plots of the evaluated models. The weak baseline was trained without any measures for normalization or augmentation and the strong baseline was trained with normalized images and online augmentations.

Additionally, we evaluated the models’ capability for domain generalization by using Uniform Manifold Approximation and Projection (UMAP) [11] plots. UMAP is a dimensionality reduction technique that can be used to visualize the high dimensional feature representations within neural networks in a two-dimensional space. For our plots, we have randomly sampled 30 patches on each WSI of the MIDOG test set and selected the output of the last layer of our RetinaNet encoders for visualization. The UMAP plot of the reference approach is visualized in Figure 3d. The data clustering independent of scanner domains shows that the domain adversarial training encouraged the extraction of domain-independent features. As a comparison Figure 3b visualizes the UMAP plot for the weak baseline. Here, the samples show a distinctive clustering according to scanner vendors. The cluster centers of the two Hamamatsu scanners are closer together, which is not surprising as they come from the same vendor and the same series (NanoZoomer). Figure 3c shows the UMAP plot of the strong baseline. Whereas the normalization and augmentation techniques pushed the distributions closer together, the GT450 still forms a distinguishable cluster at the lower right of the feature representation. Recalling the scanner-wise model performance summarized in Table 1, however, this did not impair the mitosis detection. Nevertheless, when comparing the bootstrapping visualizations in Figure 3c and Figure 3d, the remaining three scanners are less distinguishable in the feature representation of the domain adversarial model which seemed to have helped the mitotic figure detection for especially the unseen scanners. Interestingly, Figure 3d shows a separated cluster on the right hand of the main cluster with patches from all scanners. A closer look at the example patches shows that these were predominantly patches with large white areas due to teared tissue or empty fat vacuoles.

Figure 4 shows two examples where the domain adversarial model significantly outperformed the strong baseline with F_1 scores of 0.8 and 0.6 for the PANORAMIC 1000 image in Figure 4a and F_1 scores of 0.6364 and 0.4286 for the Hamamatsu RS image in Figure 4b. The large differences in performance could mainly be attributed to a higher number of false-positive predictions for the baseline model. Both examples show very intense staining which might not have been met with the augmentation methods used during training and thereby challenged the strong baseline model.

4 Conclusion

In this work, we presented our baseline algorithm for the MIDOG challenge, based on domain adversarial training. With an F_1 score of 0.7183, the algorithm is in line with previous mitotic figure algorithms trained and tested on breast cancer images from the same domain [5]. The domain adversarial training improved especially the generalization across unseen scanner domains while maintaining a similar performance on seen domains. The feature representation as UMAP plots visualizes the successful extraction of domain invariant features of the proposed network. In total, 17 algorithms were submitted to the MIDOG

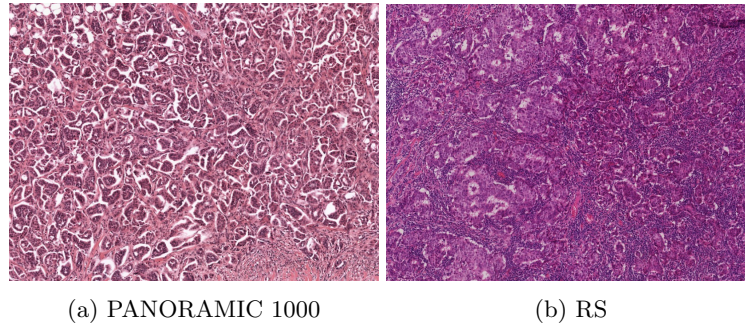


Fig. 4: Exemplary images where F_1 scores for the strong baseline and the domain adversarial varied significantly.

challenge for evaluation on the final test set. From these, four approaches outperformed this strong but out-of-competition reference approach. The code used for implementing and training the proposed network is publicly available in our GitHub² repository.

References

1. Aubreville, M., Bertram, C., Veta, M., Klopffleisch, R., Stathonikos, N., Breining, K., ter Hoeve, N., Ciompi, F., Maier, A.: Mitosis domain generalization challenge. Zenodo, doi: 10.5281/zenodo.4573978 (2021)
2. Aubreville, M., Bertram, C., Veta, M., Klopffleisch, R., Stathonikos, N., Breining, K., ter Hoeve, N., Ciompi, F., Maier, A.: Quantifying the scanner-induced domain gap in mitosis detection. *Medical Imaging with Deep Learning* (2021)
3. Aubreville, M., Bertram, C.A., Marzahl, C., Gurtner, C., Dettwiler, M., Schmidt, A., Bartenschlager, F., Merz, S., Fragoso, M., Kershaw, O., et al.: Deep learning algorithms out-perform veterinary pathologists in detecting the mitotically most active tumor region. *Sci Rep* **10**(16447), 1–11 (2020)
4. Aubreville, M., Bertram, C.A., Stathonikos, N., Veta, M., Donovan, T., ter Hoeve, N., Ciompi, F., Marzahl, C., Wilm, F., Breining, K., Maier, A., Klopffleisch, R.: MITosis DOMain Generalization Challenge (MICCAI- MIDOG 2021) Training Data. Zenodo, doi: 10.5281/zenodo.4643381 (Apr 2021)
5. Bertram, C.A., Veta, M., Marzahl, C., Stathonikos, N., Maier, A., Klopffleisch, R., Aubreville, M.: Are pathologist-defined labels reproducible? Comparison of the TUPAC16 mitotic figure dataset with an alternative set of labels. In: *Interpretable and Annotation-Efficient Learning for Medical Image Computing*, pp. 204–213. Springer (2020)
6. Ganin, Y., Lempitsky, V.: Unsupervised domain adaptation by backpropagation. In: *International conference on machine learning*. pp. 1180–1189. PMLR (2015)
7. Lafarge, M.W., Pluim, J.P., Eppenhof, K.A., Moeskops, P., Veta, M.: Domain-adversarial neural networks to address the appearance variability of histopathology images. In: *Deep learning in medical image analysis and multimodal learning for clinical decision support*, pp. 83–91. Springer (2017)

² <https://github.com/DeepPathology/MIDOG>

8. Lin, T.Y., Goyal, P., Girshick, R., He, K., Dollár, P.: Focal loss for dense object detection. In: Proceedings of the IEEE international conference on computer vision. pp. 2980–2988 (2017)
9. Macenko, M., Niethammer, M., Marron, J.S., Borland, D., Woosley, J.T., Guan, X., Schmitt, C., Thomas, N.E.: A method for normalizing histology slides for quantitative analysis. In: 2009 IEEE International Symposium on Biomedical Imaging: From Nano to Macro. pp. 1107–1110. IEEE (2009)
10. Marzahl, C., Aubreville, M., Bertram, C.A., Stayt, J., Jasensky, A.K., Barten-schlager, F., Fragoso-Garcia, M., Barton, A.K., Elsemann, S., Jabari, S., et al.: Deep learning-based quantification of pulmonary hemosiderophages in cytology slides. *Scientific Reports* **10**(1), 1–10 (2020)
11. McInnes, L., Healy, J., Melville, J.: Umap: Uniform manifold approximation and projection for dimension reduction (2020)
12. Meuten, D., Moore, F., George, J.: Mitotic count and the field of view area: time to standardize (2016)
13. Pasqualino, G., Furnari, A., Signorello, G., Farinella, G.M.: An unsupervised domain adaptation scheme for single-stage artwork recognition in cultural sites. *Image and Vision Computing* **107**, 104098 (2021)
14. Tellez, D., Balkenhol, M., Karssemeijer, N., Litjens, G., van der Laak, J., Ciompi, F.: H and E stain augmentation improves generalization of convolutional networks for histopathological mitosis detection. In: Medical Imaging 2018: Digital Pathology. vol. 10581, p. 105810Z. International Society for Optics and Photonics (2018)